Structural and thermodynamic characterization of the adrenodoxin-like domain of the electron-transfer protein Etp1 from *Schizosaccharomyces pombe*

Jürgen J. Müller, Frank Hannemann, Burkhard Schiffler, Kerstin M. Ewen, Reinhard Kappl, Udo Heinemann, and Rita Bernhardt

Published in final edited form as:
Journal of Inorganic Biochemistry. 2011 July ; 105 (7): 957-965 | doi: 10.1016/j.jinorgbio.2011.04.001
Elsevier (The Netherlands) ►

STRUCTURAL AND THERMODYNAMIC CHARACTERIZATION OF THE ADRENODOXIN-LIKE DOMAIN OF THE ELECTRON-TRANSFER PROTEIN ETP1 FROM *SCHIZOSACCHAROMYCES POMBE**

Jürgen J. Müller[a 1], Frank Hannemann[b 1], Burkhard Schiffler[b], Kerstin M. Ewen[b], Reinhard Kappl[c], Udo Heinemann[a d *], and Rita Bernhardt[b *]

[a] Max-Delbrück-Centrum für Molekulare Medizin, Berlin, Germany;
[b] FR 8.3 - Biochemie, Universität des Saarlandes, Saarbrücken, Germany,
[c] FR 2.5 - Biophysik, Universität des Saarlandes, Saarbrücken, Germany
[d] Institut für Chemie und Biochemie, Freie Universität, Berlin, Germany;

[1] J.J.M. and F.H. are common first authors.

[*]Corresponding authors:
Rita Bernhardt, Tel.: 49-681-302-3005; e-mail: ritabern@mx.uni-saarland.de
Udo Heinemann Tel.: 9406-3420 e-mail: heinemann@mdc-berlin.de

Abstract

The protein Etp1 of *Schizosaccharomyces pombe* consists of an amino-terminal COX15-like domain and a carboxy-terminal ferredoxin-like domain, Etp1^{fd}, which is cleaved off after mitochondrial import. The physiological function of Etp1^{fd} is supposed to lie in the participation in the assembly of iron-sulfur clusters and the synthesis of heme A. In addition, the protein was shown to be the first microbial ferredoxin being able to support electron transfer in mitochondrial steroid hydroxylating cytochrome P450 systems *in vivo* and *in vitro*, replacing thereby the native redox partner, adrenodoxin. Despite a sequence similarity of 39% and the fact that fission yeast is a mesophilic organism, thermodynamic studies revealed that Etp1^{fd} has a melting temperature more than 20 °C higher than adrenodoxin. The three-dimensional structure of Etp1^{fd} has been determined by crystallography. To the best of our knowledge it represents the first three-dimensional structure of a mitochondrial ferredoxin. The structure-based sequence alignment of Etp1^{fd} with adrenodoxin yields a rational explanation for their observed mutual exchangeability in the cytochrome P450 system. Analysis of the electron exchange with the *S. pombe* redox partner Arh1 revealed differences between Etp1^{fd} and adrenodoxin, which might be linked to their different physiological functions in the mitochondria of mammals and yeast.

Keywords: crystal structure; electron transfer; iron-sulfur protein; protein folding; ferredoxin reductase; iron-sulfur-cluster synthesis; ferredoxin; *Schizosaccharomyces pombe*

1. Introduction

Ferredoxins are iron-sulfur proteins which transfer electrons in several physiologically important processes such as photosynthesis, respiration and steroid biosynthesis. They are also involved in the iron-sulfur cluster assembly in different organisms like bacteria, yeast and mammals. In fission yeast (*Schizosaccharomyces pombe*) the ferredoxin Etp1^{fd} is synthesized as the C-terminal part of the protein Etp1, which is comprised of two domains with homology to human proteins. The sequence of the approximately 400 N-terminal amino acids shows significant similarity to the COX15 protein [1, 2], and the C-terminal 127 residues are clearly homologous to vertebrate-type ferredoxins [3]. Whereas COX15 is a subunit of the membrane-embedded cytochrome *c* oxidase complex and functions in the respiratory chain, Etp1^{fd} is cleaved off during mitochondrial import [3] and serves in the matrix as electron transfer protein. Moreover, an involvement of COX15 together with Etp1^{fd} and the putative Etp1^{fd} reductase Arh1 in the hydroxylation of heme O to heme A in the mitochondria of *S. pombe* has been proposed [4, 5]. This assumption was supported by a comprehensive microscopic study of the ORFeome project in fission yeast [6], which determined a mitochondrial localization of both electron transfer proteins, Arh1 and Etp1^{fd}. Very recently, we demonstrated that the ferredoxin reductase Arh1 acts, in fact, as autologous electron donor of Etp1^{fd} and that both proteins together provide mammalian class I cytochromes P450 with reduction equivalents *in vivo* and *in vitro* [3, 7].

Arh1 and Etp1^{fd} function in this case as electron carriers in heterologous vertebrate redox systems containing human CYP11B1 and CYP11B2, thus enabling the conversion of 11-deoxycortisol to cortisol and 11-deoxycorticosterone to aldosterone in fission yeast. The system thereby provides the basis for a possible application of fission yeast in biotechnological processes to produce steroid hormones [8]. So far, Etp1^{fd} is the only known microbial homologue, which can substitute adrenodoxin (Adx) as electron carrier to support the vital steps in steroid biosynthesis, but it has, in all probability, an alternative physiological function in yeast mitochondria, because *S. pombe* does not express genes encoding endogenous mitochondrial cytochromes P450 that could act as terminal electron acceptors. The homologous proteins in *Saccharomyces cerevisiae,* the [2Fe-2S] ferredoxin Yah1 and Arh1, are described on the cellular level to play an important role in heme A synthesis [4, 5] as well as in mitochondrial iron-sulfur cluster assembly on the scaffold protein Isu1 [9, 10]. These

observations were made with yeast strains containing mutants of the relevant genes and led to the proposal of a general mechanism for both processes, whereas a detailed investigation of the chemical mechanism using purified ferredoxin and ferredoxin reductase is still missing for both yeasts. However, in case of *S. pombe,* a protein crosslinking study indicated that $Etp1^{fd}$ closely interacts with the key component of iron-sulfur cluster assembly, Isu1 [11, 12].

So far, no crystal structure of an eukaryotic adrenodoxin-type ferredoxin involved in heme A synthesis and assembly of iron-sulfur clusters has been described, whereas three structures of bacterial proteins with corresponding function are already solved [13-16]. The corresponding *E. coli* ferredoxin gene was shown to be crucial for the efficient biosynthesis of Fe-S clusters *in vivo* [17, 18], and the encoded protein was proven to support *in vitro* assembly of Fe-S clusters [19]. To elucidate the functional role of this type of ferredoxins in eukaryotes, particularly in mitochondria of the model organism fission yeast, we crystallized a truncated version of the adrenodoxin-type ferredoxin, $Etp1^{fd}$(516-618) with 103 amino acids, in analogy to the previously characterized crystal structure of the truncated adrenodoxin Adx(4-108) [20]. Here, we describe the structural, thermodynamic and functional properties of $Etp1^{fd}$ in comparison with bovine Adx.

2. Experimental

2.1 Cloning, gene expression and protein purification

Expression of the full-length Etp1^{fd} (127 amino acid residues) using *E. coli* strain BL21 as expression host has been described recently [21]. Because crystallization trials failed with the full-length Etp1^{fd}, an expression construct for a truncated protein was generated in strict analogy to the previously crystallized construct Adx(4-108).

Therefore, the expression vector pTrc99a containing the cDNA coding for the ferredoxin domain of Etp1 (amino acids 505-631) served as PCR template to produce a shortened cDNA coding for the amino acids 516-618. This truncated version of Etp1^{fd} contains the amino acid variation D589N and was termed Etp1^{fd}(516-618) throughout the text. The PCR product of Etp1^{fd}(516-618) was also cloned in the vector pTrc99a and expressed in *E. coli* BL21. The gene was expressed at 37 °C in nutrient broth medium (peptone meat 5 g/l, peptone gelatin 5 g/l, peptone casein 7 g/l, yeast extract 3 g/l, sodium chloride 5 g/l) for 24 h after induction with IPTG. The soluble cell content, obtained after sonication and centrifugation, was subjected to ion exchange chromatography on a DEAE column and size exclusion chromatography on a Sephadex G-50 column. Collected fractions were analyzed spectrophotometrically for their Etp1^{fd} content. Fractions with a Q-value (A_{415}/A_{276}) higher than 0.85 were harvested, concentrated to a final concentration of 1 mM using Centriprep 10 (Amicon; Berverly, MA), and stored at -20 °C until use.

Recombinant Adx, Etp1^{fd} and Arh1 were purified as described [7, 21, 22]. The protein concentrations were calculated with ε_{414} = 9.8 (mM cm)$^{-1}$ for Etp1^{fd} [21] and Adx with ε_{450} = 11.3 (mM cm)$^{-1}$ for Arh1 [7].

2.2 Electrospray time-of-flight mass spectrometry-

The mass of Etp1^{fd}(516-618) and Etp1^{fd}(505-631) was determined by electrospray ionization (ESI) mass spectrometry using a Q-TOF1 mass spectrometer (Micromass, Manchester, UK) with an accuracy of 0.01%. For mass measurements, aliquots of the desalted Etp^{fd}(516-618) solution were dried in a vacuum centrifuge and dissolved in a (50:49:1) mixture of methanol, water and formic acid.

2.3 EPR spectroscopy

EPR spectra were recorded on a Bruker ESP300 spectrometer (X-band, 9.5 GHz) equipped with a continuous-flow helium cryostat ESR 900 and an ITC 4 temperature controller (Oxford Instruments) at 20 K. Parameters in standard measurements were: modulation frequency, 100 kHz; microwave power, 2 mW; modulation amplitude, 5 G; time constant, 41 ms. The microwave frequency was measured by a HP 5350B frequency counter. The samples after reduction with dithionite were transferred in EPR quartz tubes (Wilmad) and frozen in liquid nitrogen.

Redox titrations were performed for Etp1^{fd}(516-618) in 200 mM potassium phosphate buffer, pH 7.0, under strictly anaerobic conditions. The titration vessel was installed in an anaerobic chamber, filled with a nitrogen (95%)-hydrogen (5%) gaseous mixture, and stirred under argon gas, purified by oxygen adsorbants (Messer Griesheim, Oxysorb). The redox potential was measured by a combined micro platinum electrode (Metrohm 6.0408.100) with an Ag/AgCl reference, calibrated against a saturated quinhydrone solution, pH 7.0. The redox potential of the system was adjusted with small additions of 10, 50 or 100 mM solutions of $Na_2S_2O_4$ or $K_3[Fe(CN)_6]$. After equilibration 150 µl of the solution were filled into EPR tubes and immediately frozen in liquid nitrogen. In order to obtain stable potentials, the following mediators were used (midpoint potentials at pH 7): potassium indigotetrasulfonate (-46 mV), indigocarmine (-125 mV), 2-hydroxynaphthoquinone (-145 mV), anthraquinone-1,5- disulfonate (-170 mV), anthraquinone-2-sulfonate (-225 mV), phenosafranine (-252 mV), safranine T (-289 mV), benzyl viologen (-311 mV), diquat dibromide (-350 mV), and methyl viologen (-440 mV). In order to obtain the midpoint potentials for the FeS centers, the intensity of the iron-sulfur signals was plotted against the measured redox potential: The fit of data points was achieved using the Nernst equation.

2.4 UV-visable (UV-vis) and CD spectroscopy

Absorption spectra in the UV-vis region were recorded at room temperature on a Shimadzu double-beam spectrophotometer UV2101PC. NADPH dependent reduction of Etp1^{fd} and Adx was performed in 100 mM potassium phosphate buffer (pH 7.4) containing 20 µM ferredoxin, 0.1 µM ferredoxin reductase and 20 µM NADPH.

Circular dichroism (CD) spectra were recorded at 20 °C on a Jasco J720 spectropolarimeter (Jasco Corporation, Tokyo, Japan) in the range between 250 and 650 nm. Samples contained 20 µM ferredoxin in 10 mM HEPES buffer (pH 7.4) in a 1 cm cuvette. Temperature-dependent measurements were carried out at a heating rate of 50 °C h^{-1} from 20 to 85 °C with a temperature increment of 0.2 °C, monitoring the decrease of the CD signal at 440 nm. T_d and H_d were calculated from CD scans using the two-state model [23] and the equation

$$Y(T) = \frac{y_f + (m_f \cdot (T/T_m) + y_U + m_U \cdot (T/T_m) \cdot \exp(\frac{-\Delta H(1-T/T_m)}{R \cdot T}}{1 + \exp(\frac{-\Delta H(1-T/T_m)}{R \cdot T}}$$

T is the absolute temperature, R the universal gas constant, T_m the temperature of half-transition, y_f and y_U are the signals of folded and unfolded state at $T = 0$, m_f and m_U set the slopes of the signals of the folded and unfolded state, and ΔH is the enthalpy change upon folding at $T = T_m$.

Urea unfolding experiments were performed with 20 µM ferredoxin solutions in 10 mM HEPES buffer (pH 7.4). Samples were adjusted to the final concentration of denaturant and incubated for 15 min at 20 °C. The parameters $\Delta G°_u$ (free energy of unfolding in the absence of denaturant), m (cooperativity of unfolding), and C_m (midpoint concentration of denaturant required to unfold half of the protein) were calculated with a nonlinear regression function as previously described [24].

2.5 Functionality of the truncated Etp1^{fd}(516-618)

In order to analyze the spectral change of the ferredoxins induced by Arh1 and NADPH 10 µM solutions of Etp1^{fd}(505-631), Etp1^{fd}(516-618), Adx(1-128) and Adx(4-108) in 50 mM potassium phosphate, pH 7.4 containing 0.05 µM Arh1 were mixed with 10 µM NADPH in aerobic and anaerobic conditions. Spectra were recorded before, immediately after NADPH addition and after an

The cytochrome *c* (Cytc) reaction was carried out as described previously [21]. The samples contained 100 µM Cytc, 0.05 µM Arh1, 0.04-4 µM Etp1^{fd}(505-631) or Etp1^{fd}(516-618) and 100 µM NADPH. The reaction buffer was 50 mM potassium phosphate, pH 7.4. The reaction was started by adding NADPH and measured at room temperature following the reduction of Cytc using ε_{550} =

20,000 M^{-1} cm^{-1}. Under the conditions employed, Cytc is in large excess, and the derived K_m and V_{max} values are essentially dependent on the interactions in the Arh1- $Etp1^{fd}$ complex.

2.6 Crystallization

Crystals of $Etp1^{fd}$(516-618) were obtained at 4 °C by the sitting-drop method using a semi-automated dispensing system [25]. The reservoir solution contained 0.04 M HEPES (pH 7.0), 1.8 M Na-citrate, 3% glycerol and was mixed 1:1 with the protein solution, 18.4 mg ml^{-1}, 20 mM potassium phosphate buffer (pH 7.4) resulting in start droplet volumes of 0.6 µl. Because the crystals were temperature sensitive and no cryocondition for data sets with resolution better than 3 Å could be found, the measurements were performed at 5 °C.

2.7 Data collection and structure determination

The crystals were mounted into polyester tubes using the Room Temperature Mounting System MicroRT (MiTeGen, Ithaca, USA). Data sets from two crystals were collected at a Rigaku rotating anode generator RU H2B Rigaku Denki, Japan) with a MARDTB 345mm imaging plate detector (MarResearch, Norderstedt, Germany). Data were processed, scaled, and merged using XDS and XSCALE [26] to 2.6 Å resolution.

Initial phases for space group $P3_221$ were obtained by molecular replacement with PHASER [27] using a model obtained from coordinates of the Adx PDB entries 1e6e, 1ayf, 1l6v and 2bt6 using the Automated Protein Modelling Server [28] after removing loop V524-E530. First rigid-body refinement of two NCS-related copies of $Etp1^{fd}$(516-618) within the asymmetric unit with REFMAC [29] resulted in R_{work} 0.50 and R_{free} 0.49. After addition of the [2Fe-2S] clusters, several runs of ARPWARP [30] and REFMAC, interrupted with manual corrections in O [31] the final R values are R_{work} 0.182 and R_{free} 0.235. The averaged atomic B value corresponds to the Wilson B factor of 56 $Å^2$. No φ/ψ angles are in the disallowed region of the Ramachandran plot. Data collection and refinement statistics are summarized in Table 1. The coordinates and diffraction amplitudes were deposited in the Protein Data Bank with accession code 2wlb.

3. Results and Discussion

3.1 Expression and functionality of Etp1^{fd}

Although it was shown previously that Etp1^{fd} is cleaved upon import into the mitochondria of fission yeast [3], it is still unclear where exactly the cleavage site is localized. Therefore, we prepared two Etp1^{fd} forms, one with a length of 127 amino acids, Etp1^{fd}(505-631) [21], and a truncated variant, Etp1^{fd}(516-618), with 103 amino acids, corresponding to the adrenodoxin variants Adx(1-128) and Adx(4-108) [32]. Both variants of Etp1^{fd} were expressed as holoproteins in *E. coli* BL21 and purified to homogeneity according to SDS-PAGE analysis. Both proteins were analyzed concerning their thermodynamic stability and ability to function as electron transfer protein together with the physiological redox partner Arh1. In addition, attempts to crystallize and determine the three-dimensional structure of these ferredoxins were performed.

The molecular masses of Etp1^{fd}(516-618) and Etp1^{fd}(505-631) determined by electrospray time-of-flight mass spectrometry (Micromass, Manchester, U.K.) were 11295.0 and 14096.0 Da, respectively, which is in good agreement with the theoretical values of 11296.6 and 14095.9 for both forms. CD, UV-vis and EPR spectra indicated that both proteins assembled as holoproteins, because the typical signals of ferredoxins due to the FeS cluster were present in all spectra recorded (Fig.1, Fig.2). The protein solutions displayed the characteristic brown color of the iron-sulfur cluster and showed Q-values (A_{415}/A_{276}) of more than 0.85 as described earlier [21]. Protein yields reached more than 20 mg l^{-1} of expression culture for both forms.

In order to analyze the ability of Etp1^{fd} to accept redox equivalents from the autologous mitochondrial redox partner Arh1, both proteins were incubated with NADPH, and changes in the absorbance spectra of the ferredoxins upon reduction were followed under aerobic and anaerobic conditions. Different samples containing catalytic amounts of Arh1 in combination with both forms of Etp1^{fd}, truncated bovine Adx(4-108), and full-length bovine Adx(1-128) were analyzed. Whereas Etp1^{fd}(516-618), Etp1^{fd}(505-631) and Adx(4-108) barely accept electrons from Arh1, even after an incubation time of 5 min and independent of the presence of oxygen, a sample of full-length bovine Adx developed, immediately after mixing, an absorbance spectrum of a completely reduced ferredoxin (Fig. 2). It is well known that in the absence of an electron acceptor the reduction of Adx leads to an

electron leakage reaction in the cytochrome P450 system [33], followed by the production of reactive oxygen species (ROS), which inactivate Adx most probably by destroying the iron-sulfur center [34]. Our results here demonstrate that Etp1^{fd}, in contrast to Adx, cannot or can hardly be reduced by the electron donor Arh1 in the absence of an electron acceptor, which indicates that this protein prevents an electron leakage and therefore the destruction of the iron-sulfur center by blocking the electron flow from the reductase to the ferredoxin under these conditions. This seems to be ensured by the rather low redox potential of Etp1^{fd}, which is closer to that of ISC ferredoxins, compared with ferredoxins in cytochrome P450 systems (Table 2). The redox potential of truncated Etp1^{fd}(516-618) was determined in this study to be -381±2 mV. The non-truncated Etp1^{fd}(505-631) has a potential of -353 mV [21], and Adx(1-128) and the truncated Adx(4-108) show values of -273 and -344 mV [35], respectively. The values show that the truncation of Etp1^{fd} results in a decrease of the redox potential as described for Adx. Considering the values of Etp1^{fd}(505-631), Etp1^{fd}(516-618) and Adx it is obvious that the low redox potential of both Etp1^{fd} forms and Adx(4-108) hinders the electron flow to the ferredoxins whereas the higher potential of Adx(1-128) allows an electron flow under the same experimental conditions. Since the redox potential is one of the main differences between ferredoxins of ISC and cytochrome P450 systems [36], we conclude that ISC systems, in general, seem to avoid electron leakage and production of destructive ROS by a low redox potential of the involved ferredoxins.

Since a direct electron transfer between the redox partners Arh1 and Etp1^{fd} is blocked to a large extent and since a physiological electron acceptor for the Etp1^{fd}-Arh1 pair is not available so far, the ability of Etp1^{fd} to receive and transfer electrons from Arh1 was analyzed in the presence of the heterologous electron acceptor Cytc. Under the applied experimental conditions, the reaction was essentially dependent on the interaction in the Arh1-Etp1^{fd} complex, and steady-state kinetic values were determined as described earlier for the redox pair Adx and AdR [37]. We could demonstrate that Etp1^{fd}(516-618) can accept electrons from Arh1 and donate them to cytochrome *c* as previously described [21]. Even the truncated version Etp1^{fd}(516-618) carrying the replacement D589N is still able to transfer electrons in this system. The V_{max} values for both variants are in the same order of

magnitude being 69.1 ± 1.1 and 65.6 ± 0.5 nmoles Cyt*c* reduced per min. The K_m values are 0.36 ± 0.02 µM and 0.038 ± 0.002 µM for Etp1^{fd}(516-618) and Etp1^{fd}(505-631), respectively.

Although Etp1^{fd} can also serve as a recombinant electron carrier for mitochondrial cytochrome P450 enzymes [3], it has obviously an alternative function in yeast, because *S. pombe* does not express any endogenous mitochondrial cytochromes P450 that could act as terminal electron acceptors. Interestingly, it was shown recently that two ferredoxins have evolved in human mitochondria, one responsible for the electron transfer in the ISC assembly with a redox potential of -342 mV, the other one responsible for the electron transfer in the cytochrome P450 system with a potential of -267 mV [38].

3.2 Thermodynamic investigation of Etp1^{fd} and determinants of the high thermostability

Since Etp1^{fd} and Adx obviously serve in different physiological processes, we were wondering whether they have different structural and thermodynamic properties. To analyze the protein stability, thermal unfolding experiments with the Etp1^{fd} variants were performed. Anaerobic conditions prevented the oxidative destruction of the [2Fe-2S] cluster during heating and allowed unfolded proteins to regain 95% of the signal intensity after renaturation compared with the original absorption spectrum. All ferredoxins were incubated at room temperature in an anaerobic chamber and refolded after 12 h. The CD signal of protein melting curves recorded at 440 nm, indicating the integrity of the [2Fe-2S] cluster, decreased in a sigmoidal manner (Fig. 1), allowing a data fit according to a two-state model. The thermal transition temperatures T_m of the variants Etp1^{fd}(505-631) and Etp1^{fd}(516-618) are 70.5 ± 0.7 °C and 65.6 ± 0.5 °C, respectively. The denaturation enthalpy of the transition determined at T_m was decreased accordingly by 21 kJ mol^{-1} in the truncated form. Surprisingly, the T_m values are unusually high for a mesophilic organism and significantly higher than the values of 48.9 ± 0.6 °C and 51.7 ± 0.4 °C reported for the corresponding full-length and truncated forms of Adx [39]. Unfolding of the Etp1^{fd} variants using increasing amounts of urea was also followed by CD spectroscopy (Fig. 3). The resulting sigmoidal unfolding curves revealed the same tendency for both forms as observed in thermal unfolding. The midpoint concentration C_m of urea required to unfold half of the variants Etp1^{fd}(505-631) and Etp1^{fd}(516-618) are 4.8 M and 4.0 M, respectively, which

indicates also a resistance against urea unusually high for a ferredoxin. The free energy of unfolding $\Delta G°_u$ was 29 ± 3 kJ mol^{-1} for Etp1^{fd}(516-618). This value is two times higher than the one determined for Adx(4-108) (15.3 kJ mol^{-1}) [39].

The C-terminal part of Adx, which was truncated in Adx(4-108), was shown to be flexible in NMR studies [40]. It was also shown that redox-dependent changes of the C-terminus not only exert an influence on the binding to the cytochrome P450 but are also responsible for the dissociation of the Adx dimer that occurs in the oxidative state [41]. Therefore, it seems to be of advantage for the physiological role of Adx that the C-terminus is flexible. The precise physiological function of the C-terminus in Etp1^{fd} has not been investigated so far, but the loss of stability of the truncated form indicates that the C-terminus of Etp1^{fd} is involved in determining the overall structural stability, which is in contrast to the function of the C-terminal part in Adx. The reason for the unusually high stability of Etp1^{fd} and the opposed stability trend observed after removal of the C-terminus compared with Adx remains obscure at present. One might speculate that different electron acceptor proteins in iron-sulfur cluster assembly and steroid biosynthesis could require such big differences. However, further studies are necessary to investigate this phenomenon.

3.3 Structural comparison of Etp1^{fd}(516-618) and Adx(4-108)

So far, no 3D structure of a yeast ferredoxin involved in iron-sulfur cluster assembly or heme A biosynthesis has been resolved. To better understand the structural basis of these important processes it is, however, of great interest to evaluate the structural determinants of these proteins. In order to resolve the three-dimensional structure of Etp1^{fd}(516-618) by molecular replacement, search models derived from putidaredoxin, terpredoxin, and *E. coli* ferredoxin were applied unsuccessfully. This came as a surprise, since the *E. coli* ferredoxin was expected to share a closely similar structure with Etp1^{fd} and serves an analogous function in iron-sulfur cluster assembly. Finally, molecular replacement trials with several modified Adx models proved successful.

The structural similarity, with root-mean-square deviations (r.m.s.d.) of 1.5 Å for C^{α} atoms (1.9 Å chain B) and 2.1 Å for all atoms (2.5 Å chain B) between the Adx search model and the final structure of Etp1^{fd}(518-618) is rather moderate, explaining the difficulties in finding a molecular replacement

solution. However, the global architectures of Etp1^{fd}(516-618) and Adx(4-108) are highly similar (Fig. 4a). The r.m.s.d. value between the C^{α} atoms of both ferredoxins, except for a short stretch of amino acids (Etp1^{fd}: H546-G554; Adx: V34-G42), is 1.1 Å. It equals the r.m.s.d. value between the two molecules of Etp1^{fd}(516-618) within the asymmetric unit of the crystal. The most prominent difference between the two Etp1^{fd}(516-618) molecules is observed in loop V524-E530 (Fig. 4c). Fitting 94 out of 101 C^{α} atoms, excluding this loop, results in an r.m.s.d. value of 0.33 Å. This value defines the threshold coordinate uncertainty set by experimental errors and crystal lattice effects.

In order to probe if the sites of functional relevance in Adx are conserved in the structure of Etp1^{fd} an alignment of both molecules was performed using the structure of a cross-linked Adx-adrenodoxin reductase (AdR) complex [42] (Fig. 5). Superposition of 31 C^{α} atoms of Etp1^{fd} (A chain), G554-H566, P580-F592 and R599-Q603, with the corresponding residues of Adx (B chain), G44-H56, I70-Y82 and R89-Q93, results in an r.m.s.d. value of 0.49 Å. That holds for fitting of Etp1^{fd}(516-618) to Adx(4-108) as well as to the C^{α} backbone of Adx within the covalently cross-linked Adx-AdR complex (PDB entry 1e6e, [43]).

The interaction sites I and II and the electron transfer site of Adx align with the following residues of Etp1^{fd}(516-618):

(i) interaction site I, E582-D589, main interaction of Adx with AdR (D72-D79) (Fig. 6a),

(ii) interaction site II, D551-E553, secondary interaction of Adx with AdR and covalent crosslinking site within the Adx-AdR complex (D39-D41) (Fig. 6c),

(iii) electron transfer site, A555-T564 and L600-C602, residues near the [2Fe-2S] cluster, A45-T54 and L90-C92 in Adx (Fig. 6b).

In the interaction site I, all acidic residues of Etp1^{fd} are aligning with the corresponding Adx residues. D583 of Etp1^{fd} may be involved in CYP11A1 binding similar to E73 of Adx, whereas the other residues may bind either to AdR or to CYP11A1 as predicted for Adx [44]. Interaction site II is somewhat more distant from the AdR surface in Etp1^{fd} than in Adx, but a slight rigid-body movement of Etp1^{fd} may close the gap. The slightly changed structure of Etp1^{fd} could be one reason for the reduced efficiency in the substrate conversion with AdR and CYP11A1 [21].

At the electron transfer site (III), the hydrogen bond between E47 of Adx and N63 of AdR [43] can also be formed to link E557 of Etp1^{fd} with N63 of AdR. N-terminally, the vicinity of the [2Fe-2S] cluster of Etp1^{fd} is significantly changed compared to Adx by a sequence gap (Fig. 7). F43 stacks within the hydrophobic core in Adx. It is replaced by E553 in Etp1^{fd}, accompanied by a switching of the residue from the inside to the outside of the protein. The F43 cavity is filled by L552 in Etp1^{fd}(516-618) (Fig. 6c). Despite the much lower hydrophobicity within its core domain (PONDR server [45], results not shown), no water filled funnel is present next to the [2Fe-2S] cluster as observed in some of the plant-type ferredoxins [46].

In order to explain the differences in the thermal stability between Etp1^{fd} and Adx, the sequences and the crystal structures of both proteins were carefully examined. Overall, the analysis revealed several stabilizing intramolecular interactions of a kind previously linked to enhanced protein stability [47] and offers an excellent explanation of the increased thermodynamic stability of Etp1^{fd}. The first source of the enhanced thermal stability of Etp1^{fd} is the high number of 6 stabilizing salt bridges at the protein surface compared to 1 salt bridge in Adx. The second stabilizing factor is a decreased number of glycines and an increased number of prolines in loops, which are indicated in Fig. 7. These replacements are likely to decrease the conformational entropy upon folding and thus stabilize the native fold [48]. A higher thermal stability is also supported by substituting uncharged polar side chains by an increased number of charged and hydrophobic residues in Etp1^{fd} and by shortening the loop between residues 550-560 in Etp1^{fd} by two amino acids. An additional factor contributing to higher thermostability is the helix dipole stabilization [49] due to the replacement of the hydrophobic Val34 in Adx by His546 in Etp1^{fd} (Figs. 4, 7).

3.4 Conclusions

It is demonstrated that Etp1^{fd} shares many structural features with bovine Adx, which explains the ability of Etp1^{fd} to replace Adx in various steroid hydroxylase systems. Analyses of the stability of Etp1^{fd} revealed that, although being isolated from a mesophilic organism, it shows unusually high stability compared with Adx. Structural and sequence data provide a rational explanation for this

behavior. In addition, a redox potential based mechanism was discovered preventing iron-sulfur-cluster destruction by avoiding the formation of reactive oxygen species by the Arh1-Etp1^{fd} complex. It needs to be investigated which consequences these observations have on the different physiological functions of Etp1^{fd} and Adx.

Abbreviations:

AdR	adrenodoxin reductase
Adx	adrenodoxin
Arh1	adrenodoxin reductase homologue 1
CD	circular dichroism
COX	cytochrome c oxidase
DEAE	diethylaminoethyl
Etp1^{fd}	electron transfer protein ferredoxin domain
Fdx	Ferredoxin
HEPES	4-(2-hydroxyethyl)-1-piperazineethanesulfonic acid
IPTG	isopropyl β-D-1-thiogalactopyranoside
ISC	iron-sulfur cluster
ORF	open reading frame
PDB	protein data bank
Pdx	Putidaredoxin

ROS	reactive oxygen species
r.m.s.d.	root-mean-square deviations

Acknowledgements

We thank A. Feske and Dr. Y. Roske for growing the crystals, Dr. Eva-Christina Müller for the mass spectrometer measurements and Wolfgang Reinle for protein purification. This work was supported by the Deutsche Forschungsgemeinschaft (grant BE1343/12-3) and the Fonds der Chemischen Industrie.

References

[1] D.M. Glerum, I. Muroff, C. Jin, A. Tzagoloff, J. Biol. Chem. 272 (1997) 19088-19094.

[2] V. Petruzzella, V. Tiranti, P. Fernandez, P. Ianna, R. Carrozzo, M. Zeviani, Genomics 54 (1998) 494-504.

[3] M. Bureik, B. Schiffler, Y. Hiraoka, F. Vogel, R. Bernhardt, Biochemistry 41 (2002) 2311-2321.

[4] M.H. Barros, C.G. Carlson, D.M. Glerum, A. Tzagoloff, FEBS Lett. 492 (2001) 133-138.

[5] M.H. Barros, F.G. Nobrega, A. Tzagoloff, J. Biol. Chem. 277 (2002) 9997-10002.

[6] A. Matsuyama, R. Arai, Y. Yashiroda, A. Shirai, A. Kamata, S. Sekido, Y. Kobayashi, A. Hashimoto, M. Hamamoto, Y. Hiraoka, S. Horinouchi, M. Yoshida, Nat. Biotechnol. 24 (2006) 841-847.

[7] K.M. Ewen, B. Schiffler, H. Uhlmann-Schiffler, R. Bernhardt, F. Hannemann, FEMS Yeast Res. 8 (2008) 432-441.

[8] C.A. Dragan, S. Zearo, F. Hannemann, R. Bernhardt, M. Bureik, FEMS Yeast Res. 5 (2005) 621-625.

[9] H. Lange, A. Kaut, G. Kispal, R. Lill, Proc. Natl. Acad. Sci. U S A 97 (2000) 1050-1055.

[10] R. Lill, Nature 460 (2009) 831-838.

[11] G. Wu, S.S. Mansy, S.P. Wu, K.K. Surerus, M.W. Foster, J.A. Cowan, Biochemistry 41 (2002) 5024-5032.

[12] S.P. Wu, G. Wu, K.K. Surerus, J.A. Cowan, Biochemistry 41 (2002) 8876-8885.

[13] T. Iwasaki, D. Ohmori, N. Shimizu, T. Kumasaka, Acta Cryst. F63 (2007) 1014-1016.

[14] Y. Kakuta, T. Horio, Y. Takahashi, K. Fukuyama, Biochemistry 40 (2001) 11007-11012.

[15] G. Sainz, J. Jakoncic, L.C. Sieker, V. Stojanoff, N. Sanishvili, M. Asso, P. Bertrand, J. Armengaud, Y. Jouanneau, J. Biol. Inorg. Chem. 11 (2006) 235-246.

[16] F. Xu, S.G. Bell, Y. Peng, E.O.D. Johnson, M. Bartlam, Z. Rao, L.L. Wong, Proteins-Structure Function and Bioinformatics 77 (2009) 867-880.

[17] U. Tokumoto, Y. Takahashi, J. Biochem. 130 (2001) 63-71.

[18] M. Nakamura, K. Saeki, Y. Takahashi, J. Biochem. 126 (1999) 10-18.

[19] F. Bonomi, S. Iametti, D. Ta, L.E. Vickery, J. Biol. Chem. 280 (2005) 29513-29518.

[20] A. Müller, J.J. Müller, Y.A. Müller, H. Uhlmann, R. Bernhardt, U. Heinemann, Structure 6 (1998) 269-280.

[21] B. Schiffler, M. Bureik, W. Reinle, E.C. Muller, F. Hannemann, R. Bernhardt, J. Inorg. Biochem. 98 (2004) 1229-1237.

[22] F. Hannemann, M. Rottmann, B. Schiffler, J. Zapp, R. Bernhardt, J. Biol. Chem. 276 (2001) 1369-1375.

[23] P.L. Privalov, Adv. Protein Chem. 33 (1979) 167-241.

[24] F. Hannemann, A.K. Bera, B. Fischer, M. Lisurek, K. Teuchner, R. Bernhardt, Biochemistry 41 (2002) 11008-11016.

[25] U. Heinemann, K. Bussow, U. Mueller, P. Umbach, Acc. Chem. Res. 36 (2003) 157-163.

[26] W. Kabsch, J. Appl. Crystallogr. 26 (1993) 795-800.

[27] R.J. Read, Acta Crystallogr. D 57 (2001) 1373-1382.

[28] T. Schwede, J. Kopp, N. Guex, M.C. Peitsch, Nucleic Acids Res. 31 (2003) 3381-3385.

[29] G.N. Murshudov, A.A. Vagin, E.J. Dodson, Acta Crystallogr. D 53 (1997) 240-255.

[30] V.S. Lamzin, K.S. Wilson, Acta Crystallogr. D 49 (1993) 129-147.

[31] T.A. Jones, J.Y. Zou, S.W. Cowan, Kjeldgaard, Acta Crystallogr. A 47 (1991).

[32] H. Uhlmann, R. Kraft, R. Bernhardt, J. Biol. Chem. 269 (1994) 22557-22564.

[33] I. Hanukoglu, Drug Metab. Rev. 38 (2006) 171-196.

[34] R. Rapoport, D. Sklan, I. Hanukoglu, Arch. Biochem. Biophys. 317 (1995) 412-416.

[35] A.V. Grinberg, F. Hannemann, B. Schiffler, J.J. Müller, U. Heinemann, R. Bernhardt, Proteins 40 (2000) 590-612.

[36] K.M. Ewen, M. Kleser, R. Bernhardt, Biochim. Biophys. Acta 1814 (2011) 111-125.

[37] H. Uhlmann, R. Bernhardt, J. Biol. Chem. 270 (1995) 29959-29966.

[38] A.D. Sheftel, O. Stehling, A.J. Pierik, H.P. Elsasser, U. Muhlenhoff, H. Webert, A. Hobler, F. Hannemann, R. Bernhardt, R. Lill, Proc. Natl. Acad. Sci. USA 107 (2010) 11775-11780.

[39] A.V. Grinberg, R. Bernhardt, Protein Eng. 11 (1998) 1057-1064.

[40] D. Beilke, R. Weiss, F. Lohr, P. Pristovsek, F. Hannemann, R. Bernhardt, H. Ruterjans, Biochemistry 41 (2002) 7969-7978.

[41] J. Behlke, O. Ristau, E.C. Müller, F. Hannemann, R. Bernhardt, Biophys. Chem. 125 (2007) 159-165.

[42] J.J. Müller, A. Lapko, G. Bourenkov, K. Ruckpaul, U. Heinemann, J. Biol. Chem. 276 (2001) 2786-2789.

[43] E.C. Müller, A. Lapko, A. Otto, J.J. Müller, K. Ruckpaul, U. Heinemann, Eur. J. Biochem. 268 (2001) 1837-1843.

[44] L.E. Vickery, Steroids 62 (1997) 124-127.

[45] P. Romero, Z. Obradovic, C. Kissinger, J.E. Villafranca, A.K. Dunker, Ieee International Conference on Neural Networks Vol. 1-4 (1997) 90-95.

[46] J.J. Müller, A. Müller, M. Rottmann, R. Bernhardt, U. Heinemann, J. Mol. Biol. 294 (1999) 501-513.

[47] M. Sadeghi, H. Naderi-Manesh, M. Zarrabi, B. Ranjbar, Biophys. Chem. 119 (2006) 256-270.

[48] C.N. Pace, U. Heinemann, U. Hahn, W. Saenger, Angew. Chem. 30 (1991) 343-360.

[49] K.M. Armstrong, R.L. Baldwin, Proc. Natl. Acad. Sci. U S A 90 (1993) 11337-11340.

[50] R.A. Laskowski, M.W. Macarthur, D.S. Moss, J.M. Thornton, J. Appl. Crystallogr. 26 (1993) 283-291.

[51] Y.S. Jung, H.S. Gao-Sheridan, J. Christiansen, D.R. Dean, B.K. Burgess, J. Biol. Chem. 274 (1999) 32402-32410.

[52] G. Mitou, C. Higgins, P. Wittung-Stafshede, R.C. Conover, A.D. Smith, M.K. Johnson, J. Gaillard, A. Stubna, E. Munck, J. Meyer, Biochemistry 42 (2003) 1354-1364.

[53] T. Okamura, M.E. John, M.X. Zuber, E.R. Simpson, M.R. Waterman, Proc. Natl. Acad. Sci. USA 82 (1985) 5705-5709.

[54] G.S. Wilson, J.C.M. Tsibris, I.C. Gunsalus, J. Biol. Chem. 248 (1973) 6059-6061.

[55] N. Collaborative Computational Project, Acta Cryst. D50 (1994) 760-763.

[56] P.J. Kraulis, J. Appl. Crystallogr. 24 (1991) 946-950.

[57] D.N. Beratan, J.N. Betts, J.N. Onuchic, Science 252 (1991) 1285-1288.

[58] W. Kabsch, C. Sander, Biopolymers 22 (1983) 2577-2637.

Table 1

X-ray data collection and refinement statistics. Values in parentheses refer to the outer shell of reflections (2.78-2.6 Å). [a]R_{merge} = $\Sigma|I-\langle I\rangle| / \Sigma I$ from two crystals. [b]$R_{free} = \Sigma||F_o|-|F_c|| / \Sigma |F_o|$, for test data set. [c]$R_{work} = \Sigma||F_o|-|F_c|| / \Sigma |F_o|$, where F_o is the observed and F_c is the structure factor amplitude calculated from the model. The sum is over all reflections. *R* for map has been calculated by using the EDS-server (eds.bmc.uu.se).Test data set is 5% of the reflections, randomly chosen.[d] [50].

Space group	$P3_221$
Resolution [Å]	20 - 2.6
Observed reflections	28197 (4858)
Independent reflections	8197 (1396)
$\langle I/\sigma(I)\rangle$	8.5 (3.4)
Averaged redundancy	3.4 (3.5)
B [Å^2], Wilson	56.1
Completeness: overall / last shell [%]	96.8 (92.4)
Mosaicity [°]	0.1
Unit cell *a* [Å] / *c* [Å]	81.96 / 68.29
R_{merge}[a] [%]: ov. / last shell	10.9 / 50.9
Amino acids chain A / chain B	516 - 618 / 518 - 618

Number all atoms / protein atoms / Fe-S / solvent	1577 / 1567 / 8 / 2
R / R_{work}[b] / R_{free}[c] [%]	18.4 / 18.2 / 23.5
R for map [%]	19.7
r.m.s.d. bond distances [Å]	0.012
r.m.s.d. bond angles [°]	1.45
Ramachandran diagram	
Most favored / addit. allowed / gener. allowed / disallowed[d] [%]	89.7 / 9.7 / 0.6 / 0.0
Mean B values main chain / side chain / all [Å^2]	50.6 / 55.9 / 53.1
Estimated overall coordinate error (R / R_{free} / ML) [Å]	0.26 / 0.28 / 0.20

Table 2

Comparison of redox potentials of ferredoxins involved either in ISC or cytochrome P450 systems.

Ferredoxin	Organism	Function	Redox potential
EcFdx [14, 19]	*Escherichia coli*	ISC system	-380 mV
AvFdx [51]	*Azotobacter vinelandii*	ISC system	-344 mV
AaFdxV [52]	*Aquifex aeolicus*	ISC system	-390 mV
HsFdx2 [38]	*Homo sapiens*	ISC system	-342 mV
Etp1^{fd} [21]	*Schizosaccharomyces pombe*	ISC system	-353 mV
BtAdx [53]	*Bos taurus*	P450 system	-274 mV
HsFdx1 [38]	*Homo sapiens*	P450 system	-267 mV
PpPdx [54]	*Pseudomonas putida*	P450 system	-235 mV

Figure legends

Fig. 1. **CD and EPR spectroscopy.** A, CD spectra of Etp1^{fd}(505-631) (black line) and Etp1^{fd}(516-618) (gray line) were recorded in the visible and near UV region. Samples consisted of 25 µM ferredoxin in 10 mM HEPES buffer (pH 7.4). B, Fitted single-wavelength thermal unfolding curves of Etp1^{fd}(505-631) in black, Etp1^{fd}(516-618) in dark gray and Adx(4-108) in light gray were recorded at 440 nm, which corresponds to the main CD signal of the iron-sulfur cluster. C) EPR spectra of Etp1^{fd}(505-631) (black line) and Etp1^{fd}(516-618) (gray line). Samples of 0.4 mM protein in 10 mM potassium phosphate buffer, pH 7.4 were reduced using sodium dithionite under an argon atmosphere in a glove box. EPR spectra were recorded on a Bruker ESP300 spectrometer. Both Etp1^{fd} forms display identical apparent g-values of g_1=2.03 and g_2=1.94 typical for vertebrate-type ferredoxins.

Fig. 2. **Reduction of ferredoxins.** Enzymatic reduction of Adx(1-128) (A), Adx(4-108) (B), Etp1^{fd}(505-631) (C) and Etp1^{fd}(516-618) (D). Spectra of ferredoxins in the oxidative state are depicted in black. Spectra of ferredoxins immediately after mixing with NADPH and Arh1 are shown in gray.

Fig. 3. **Urea unfolding of Etp1^{fd}(505-631) and Etp1^{fd}(516-618).** CD spectra of Etp1^{fd}(505-631) (A) and Etp1^{fd}(516-618) (C) were recorded in the visible and near UV region at urea concentrations between 0 and 8 M. In both A and C, the CD signals have the maximum between 0 and 2M and minimum intensities with 8 M urea concentrations, respectively. Urea unfolding of Etp1^{fd}(505-631) (B) and Etp1^{fd}(516-618) (D) was plotted using data derived from the CD signal at 450 nm, see (A, C).

Fig. 4. **Crystal structures of Etp1^{fd}(516-618) and of Adx(4-108) from PDB entry 1ayf.** Essential functional side chains are labeled and shown in ball-and-stick representation. Etp1^{fd}(516-618) chain A is shown in dark yellow (A) and Adx(4-108) chain A in blue. C) Superposition of Etp1^{fd}(516-618) chains A, dark yellow, and B, black) and Adx(4-108) (blue) (stereo view). The structurally conserved and functionally relevant peptides (44-56, 70-82, 89-93) of Adx were superimposed with the

corresponding peptides of Etp1^{fd} (554-566, 580-592, 599-603) using the program LSQKAB [55]. The residues discussed in text are shown for Adx (sticks), and for Etp1^{fd} (ball-and-stick). Conserved hydrogen bonds are shown as dotted lines. The black arrow marks the loop V524-E530 of Etp1^{fd}(516-618) chain B.

Fig. 5. **Superposition of functional residues from Etp1^{fd} and Adx in complex with AdR.** Functional residues from Etp1^{fd}(516-618) (C^{α} trace colored dark yellow) and Adx (C^{α} trace colored blue) are depicted within the covalently crosslinked Adx·AdR complex [42], PDB entry 1e6e. The reductase is depicted as a secondary structure plot with the NADP and FAD moieties in ball-and-stick representation [56].

Fig. 6. **Superposition of functionally important residues.** Stereo view of the superposition of functionally important residues in the interaction site I (A), electron transfer site (B), and interaction site II (C) of Etp1^{fd}(516-618) and Adx within the Adx·AdR complex (1e6e). AdR residues are colored gray, Etp1^{fd} yellow, and Adx blue. Hydrogen bonds between AdR and Adx are shown with dotted lines [42]. A predicted electron transfer pathway from FAD to [2Fe-2S] is indicated by red covalent bonds and dotted lines in 6B (calculated with HARLEM, [57]).

Fig. 7. **Sequence and secondary structure alignment**. Sites influencing thermal stability are marked in the alignment of bovine Adx(4-108) and Etp1^{fd}(516-618). The extended loop in Adx is highlighted cyan, and stabilizing prolines in Etp1^{fd} loops are colored cyan. The V34 to H546 exchange accompanied with helix dipole moment enhancement in Etp1^{fd} is marked by a blue bar. Charge changes are indicated by correspondingly colored bars (red – negative charge, blue – positive charge). The red lines are salt bridges in Etp1^{fd} additional to the internal bridge in Adx and Etp1^{fd} (colored magenta). The secondary structure of Adx(4-108) and Etp1^{fd}(516-618) was analyzed using the program DSSP [58], green arrows mark β-strands, α-helices are symbolized by brown spirals.

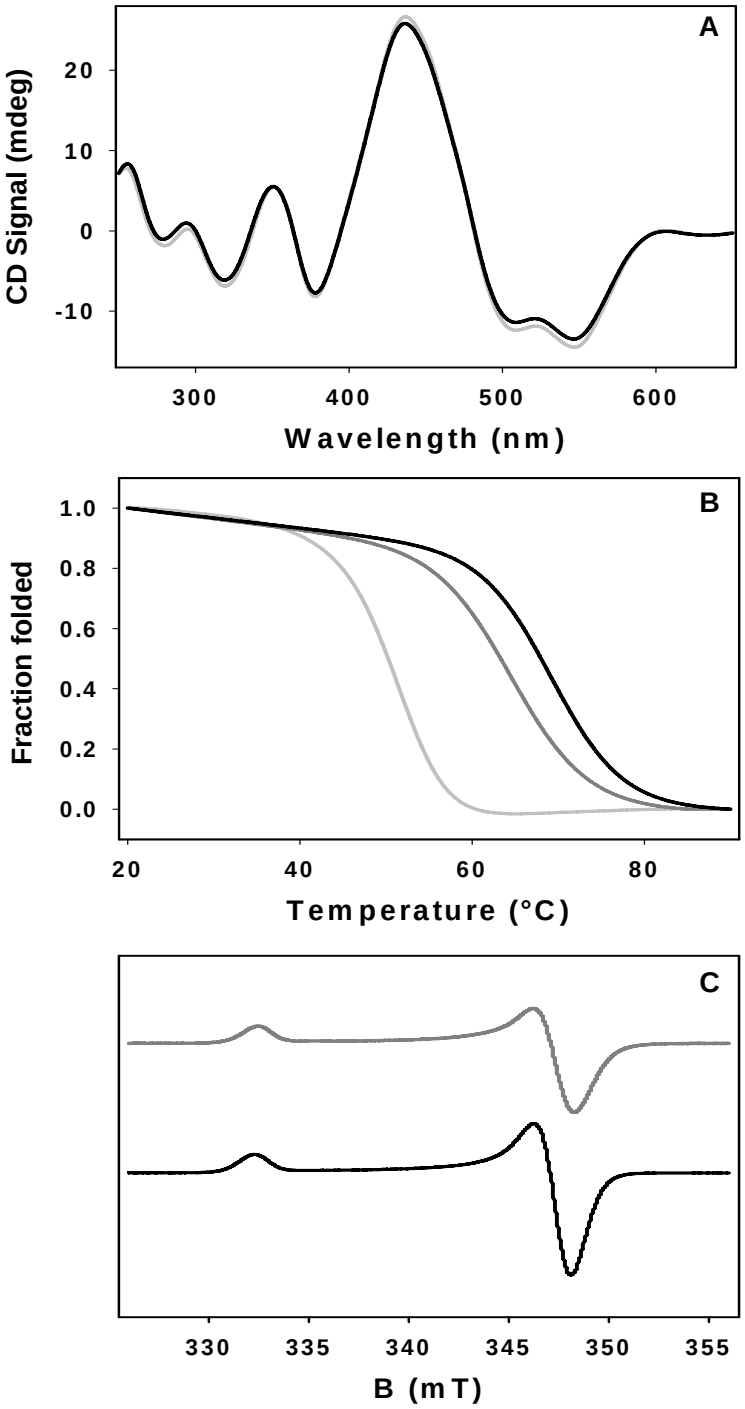
A
CD Signal (mdeg)
20
10
0
-10
300
400
500
600
Wavelength (nm)
B
Fraction folded
1.0
0.8
0.6
0.4
0.2
0.0
20
40
60
80
Temperature (°C)
C
330
335
340
345
350
355
B (mT)

Figure 1

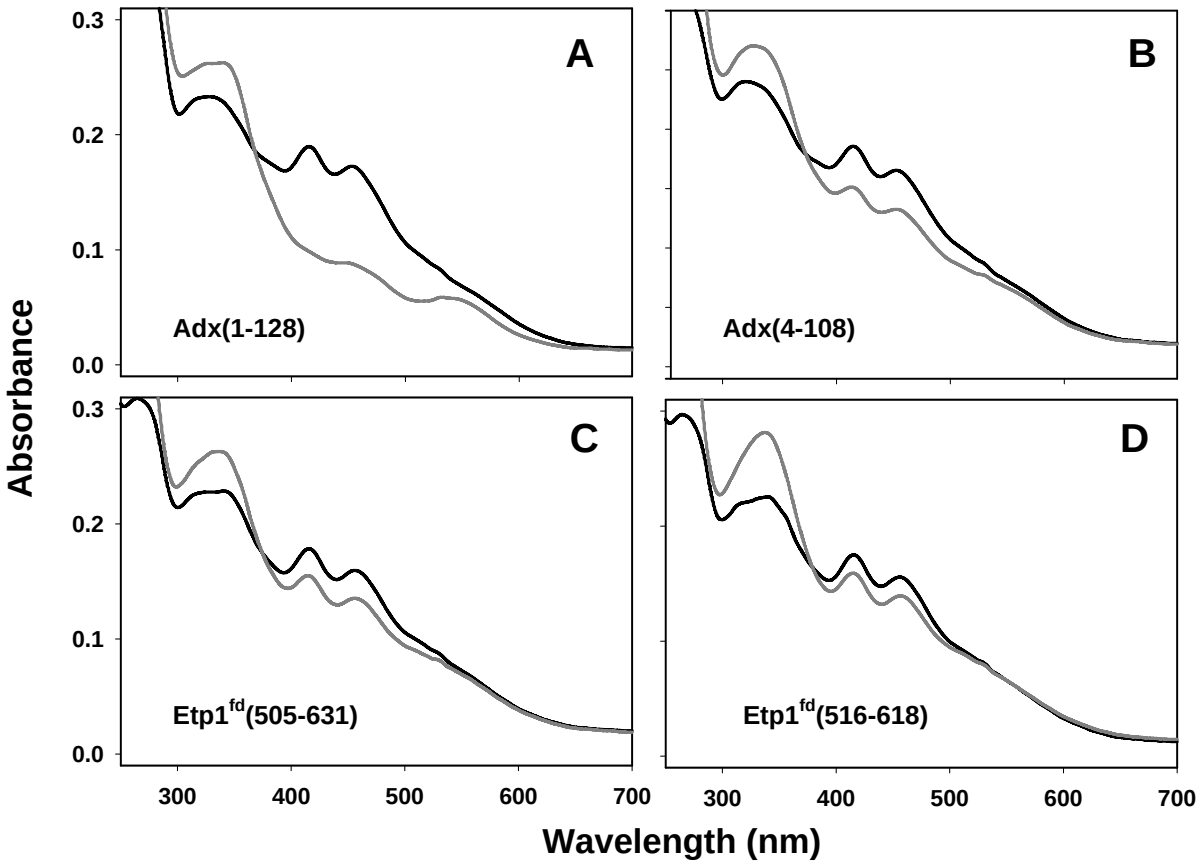
A
B
C
D
Adx(1-128)
Adx(4-108)
Etp1fd(505-631)
Etp1fd(516-618)
Absorbance
Wavelength (nm)
0.0
0.1
0.2
0.3
300
400
500
600
700

Figure 2

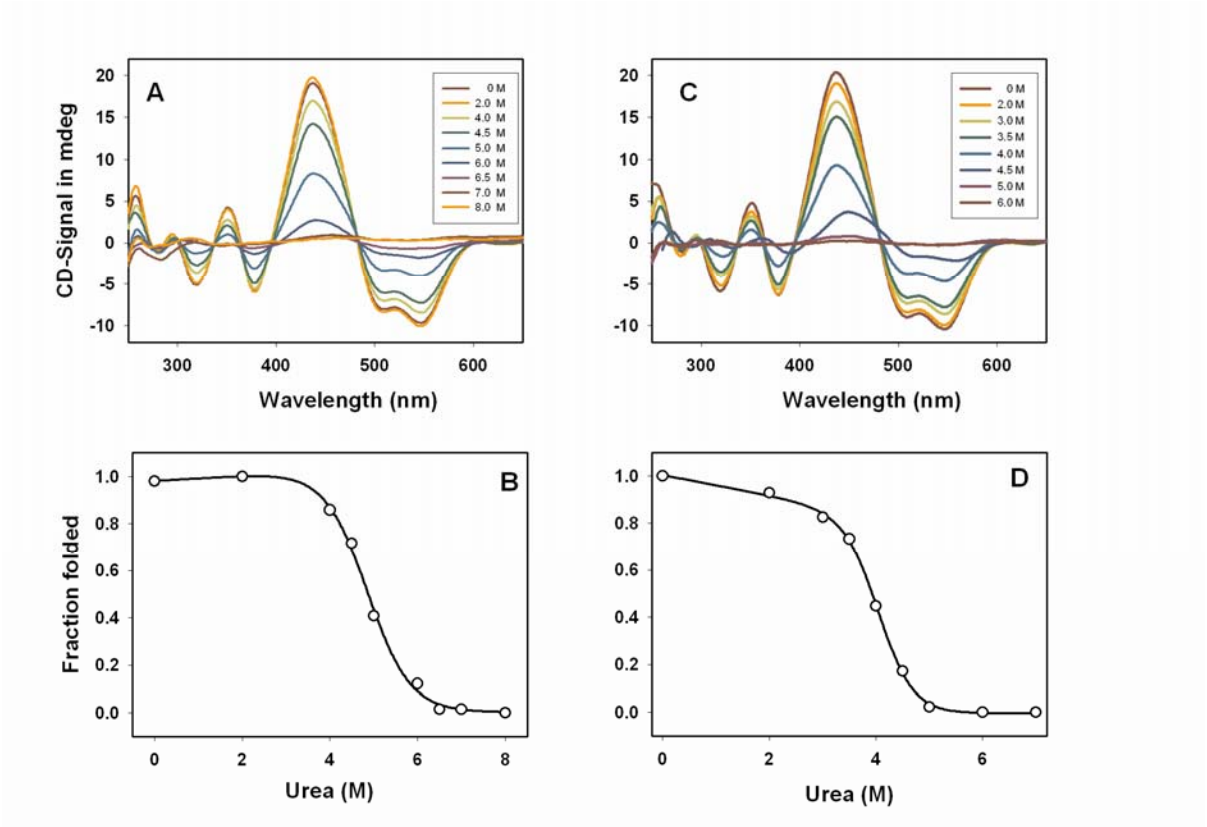
A
CD-Signal in mdeg
Wavelength (nm)
0 M
2.0 M
4.0 M
4.5 M
5.0 M
6.0 M
6.5 M
7.0 M
8.0 M
C
Wavelength (nm)
0 M
2.0 M
3.0 M
3.5 M
4.0 M
4.5 M
5.0 M
6.0 M
B
Fraction folded
Urea (M)
D
Urea (M)

Figure 3

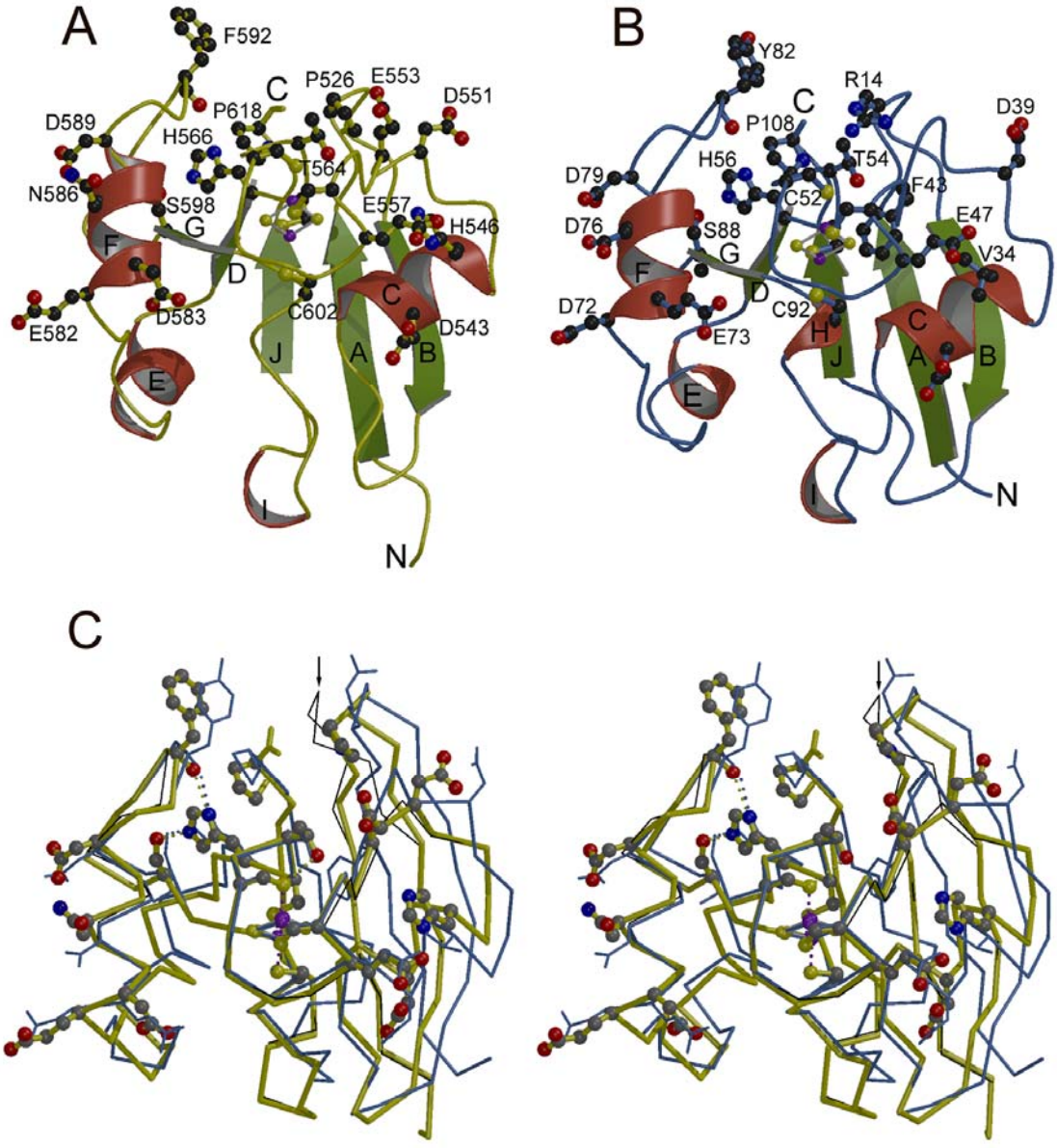
A
F592
C
P526
E553
D551
P618
D589
H566
T564
N586
S598
G
E557
H546
F
D
C
D583
C602
D543
E582
J
A
B
E
I
N
B
Y82
R14
C
D39
P108
H56
T54
D79
C52
F43
D76
S88
E47
G
V34
F
D
D72
C92
H
C
E73
J
A
B
E
I
N
C

Figure 4

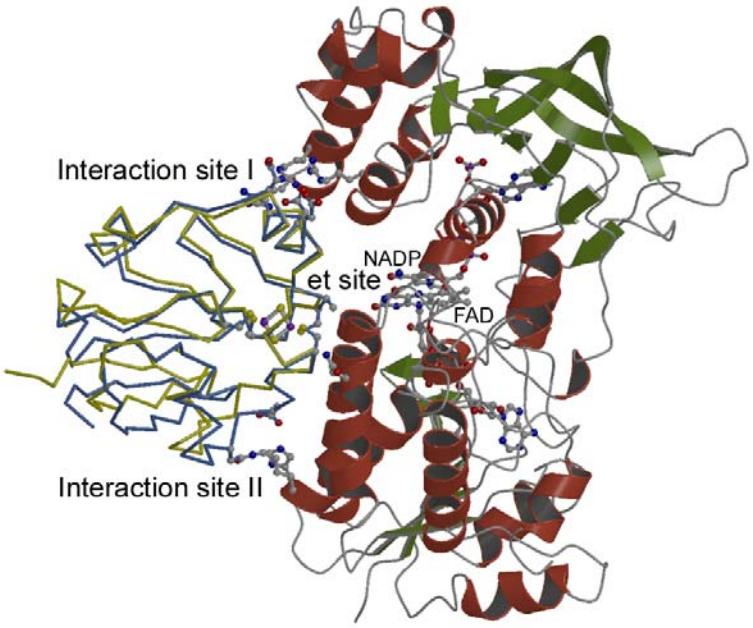

Figure 5

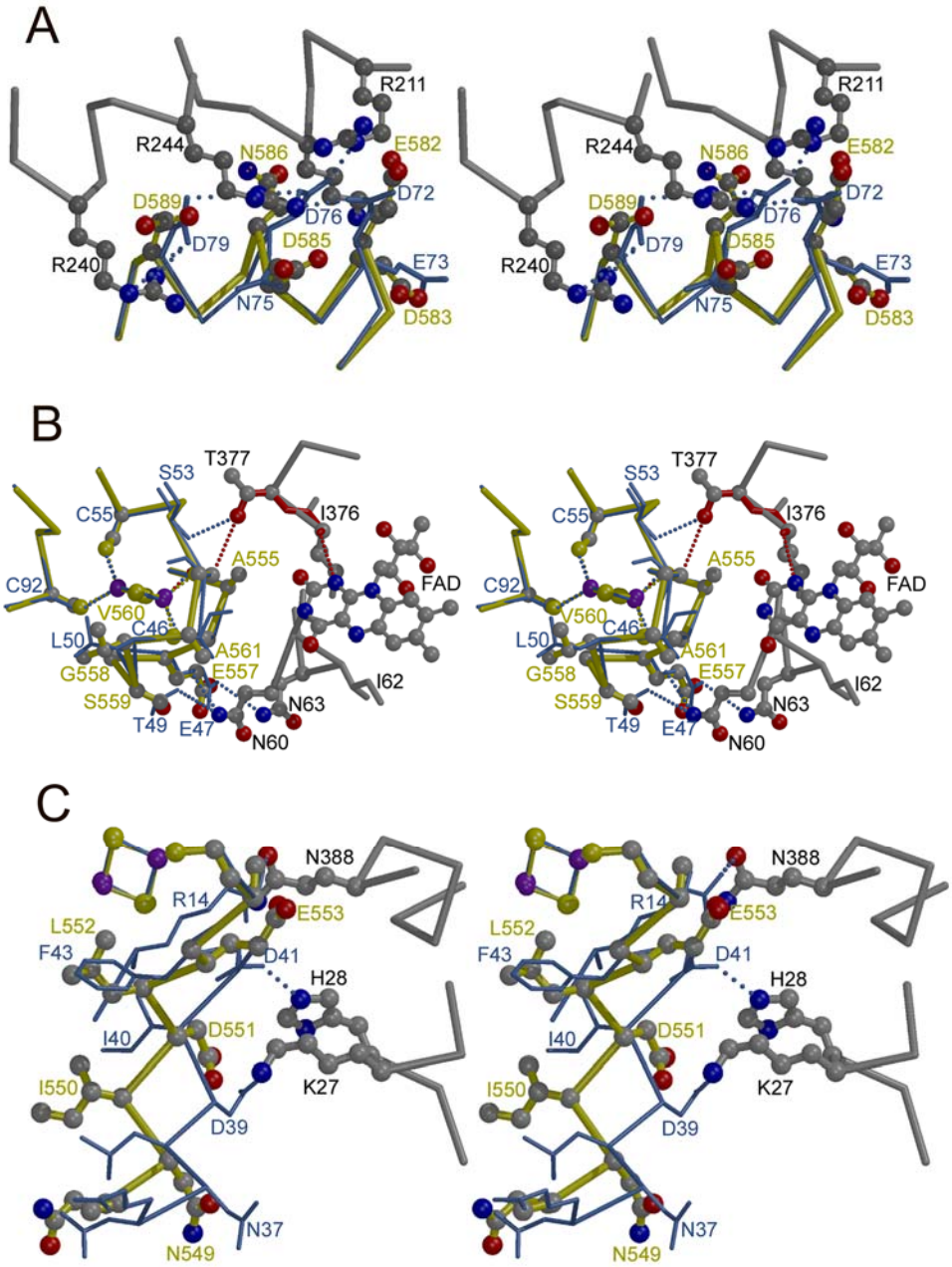
A
R211
R244
N586
E582
D589
D72
D76
D79
D585
R240
E73
N75
D583
B
T377
S53
C55
I376
A555
C92
FAD
V560
C46
L50
A561
G558
E557
I62
S559
N63
T49
E47
N60
C
N388
R14
E553
L552
F43
D41
H28
I40
D551
I550
K27
D39
N37
N549

Figure 6

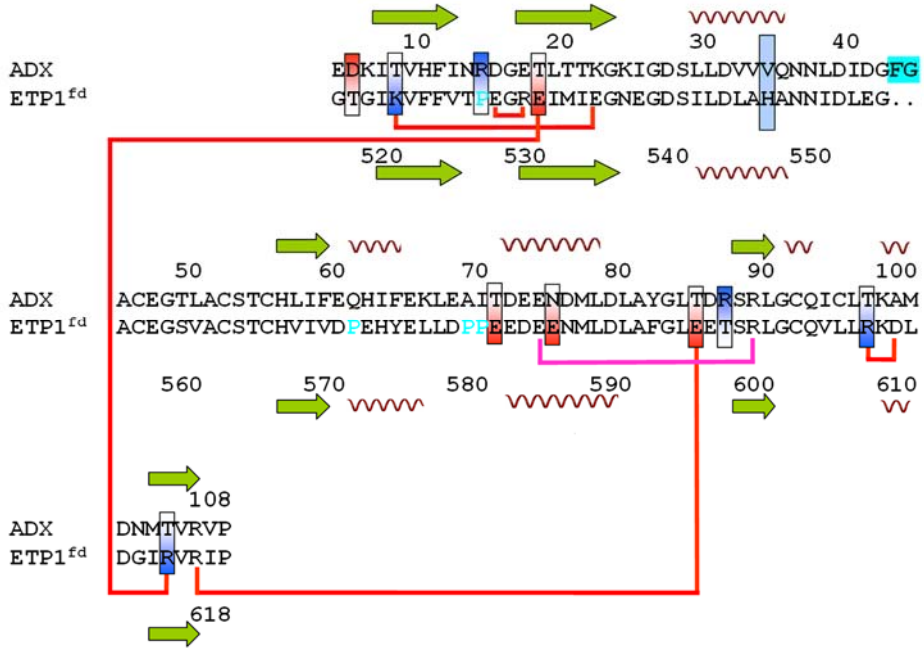
10
20
30
40
ADX
ETP1fd
520
530
540
550
50
60
70
80
90
100
ADX
ETP1fd
560
570
580
590
600
610
108
ADX
ETP1fd
618

Figure 7